Journal of Computational Physics **170,** 742–763 (2001)
doi:10.1006/jcph.2001.6759, available online at http://www.idealibrary.com on IDEAL®

The Numerical Methods for Oscillating Singularities in Elliptic Boundary Value Problems

Hae-Soo Oh,*[,1] Hoonjoo Kim,†[,2] and Sung-Jin Lee‡[,3]

*Department of Mathematics, University of North Carolina at Charlotte, Charlotte, North Carolina 28223-0001; †Department of Computer Science, Daebul University, Youngam, Korea; and ‡Department of Mathematics, Daejin University, Pochun, Korea

E-mail: hso@uncc.edu, hoonjoo@daebul.daebul.ac.kr, hyper@road.daejin.ac.kr

Received July 28, 2000; revised February 14, 2001

The singularities near the crack tips of homogeneous materials are monotone of type r^α and $r^\alpha \log^\delta r$ (depending on the boundary conditions along nonsmooth domains). However, the singularities around the interfacial cracks of the heterogeneous bimaterials are oscillatory of type $r^\alpha \sin(\varepsilon \log r)$. The method of auxiliary mapping (MAM), introduced by Babuška and Oh, was proven to be successful in dealing with r^α type singularities. However, the effectiveness of MAM is reduced in handling oscillating singularities. This paper deals with oscillating singularities as well as the monotone singularities by extending MAM through introducing the power auxiliary mapping and the exponential auxiliary mapping.

Key Words: monotone singularity; oscillating singularity; interfacial cracks; elliptic boundary value problems; the p-version (the h-p Version) of finite element method; method of auxiliary mapping; the power (the Exponential) auxiliary mapping.

1. INTRODUCTION

This paper studies an effective new method that yields highly accurate finite element solutions for elliptic boundary value problems containing the singularities of types r^α, $r^\alpha \log^\delta r$, or $r^\alpha \sin(\varepsilon \log r)$, where $0 < \alpha < 1$. These singularities are usually caused by either the nonsmoothness of data (such as jump boundary conditions or singular loads) or the nonsmoothness of the solution domain (such as corners or cracks) [10, 19].

[1] This research is supported in part by NSF grant INT-9722699.

[2] This work is supported in part by the KOSEF Postdoctoral Fellowship and Daebul University, Korea.

[3] This work is supported in part by the KOSEF Postdoctoral Fellowship and Daejin University, Korea.

0021-9991/01 $35.00

The accuracy of the finite element solution depends on the regularity of the true solution of the problem concerned. In the presence of singularities, the true solution has a low regularity and hence it is difficult for FEM to yield an accurate economical solution. In theory and practice of FEM, considerable effort has been made to design special approaches dealing with elliptic boundary value problems containing singularities. In the case of nonsmoothness of the solution domains, the following approaches are the most typical: mesh refinement [1, 6, 11], use of special elements [2, 15, 24], use of the enriched (nonlocal) basis functions [12, 22].

Babuška and Oh [5, 17, 18] introduced a new method, the method of auxiliary mapping (MAM), which can effectively handle the r^α type singularities [14]. This paper takes this method, MAM, and makes several extensions. One such extension introduces the exponential auxiliary mapping to effectively deal with $r^\alpha \log^\delta r$-type and $r^\alpha \sin(\varepsilon \log r)$-type singularities. The essence of this method involves locally transforming a neighborhood Ω_S of each singularity point to a new domain $\hat{\Omega}_S$ by using mappings such as $z = \zeta^\beta$ (the power auxiliary mapping) and $z = e^{\beta_1\xi + i\beta_2\eta}$ (the exponential auxiliary mapping). Here $z = x + iy$, $\zeta = \xi + i\eta$, β is directly determined by the known nature of the singularity in such a way which locally transforms the exact (singular) solution to a smoother function. This can be easily approximated in the new mapped domain by the conventional use of the p-version of the FEM. In practice, the mapping size β is recommended to be slightly larger than $1/\alpha$ for the power auxiliary mapping. For example, consider a crack singularity of the form $r^{1/2} f(r, \theta)$ located at the origin, where f is smooth. Then the auxiliary mapping $\psi(z) = z^{1/4}$ maps the upper half plane into one half of the first quadrant, and a point $(\hat{r}, \hat{\theta})$ in the lower half of the first quadrant evaluates as $(\hat{r})^2 f((\hat{r})^4, 4\hat{\theta})$, a smooth function.

To further understand the effect of the power auxiliary mapping $\psi(z) = z^{1/4}$, let $\Omega_S = \{(r, \theta) : r < R_1, 0 \le \theta \le \pi/4\}$. Then, $\hat{\Omega}_S = \psi(\Omega_S) = \{(\hat{r}, \hat{\theta}) : \hat{r} \le R_1^{1/4}, 0 \le \hat{\theta} \le \pi/16\}$. If we consider the basis function of p-degree 12 over $\hat{\Omega}_S$, the singular functions created over Ω_S through the power auxiliary mapping restricted to the positive x-axis are generated by $\{1, x^{1/4}, x^{1/2}, x^{3/4}, x, x^{5/4}, \ldots, x^{11/4}, x^3\}$. That is, the auxiliary mapping implicitly creates special singular basis functions which mimic the singularity. However, unlike other singular function approaches, the method introduced in this paper does not require constructing or using singular basis functions in actual computations.

This paper is organized as follows: Section 2 develops the new method, MAM, by introducing two auxiliary mappings: the power auxiliary mapping and the exponential auxiliary mapping. Section 3 tests this method with respect to singular functions that contain various types of singularities. For a clearer presentation of the method, proofs of lemmas, used in theory development and numerical experiments, can be found in the Appendix.

For brevity, the theory and numerical results are presented with respect to elliptic boundary value problems. However, the method is applicable to elasticity problems for their finite element analysis (see [16, 18]).

2. THE METHOD OF AUXILIARY MAPPING TO DEAL WITH SINGULARITIES

In this section, by introducing the exponential auxiliary mapping and the power auxiliary mapping, MAM is modified and extended so that it may handle the oscillating singularities as well as the monotone singularities.

2.1. *A Model Problem*

In this paper, Ω is a simply connected open subset of the plane $\mathbf{R}^2$ such that its closure $\bar{\Omega}$ is a nonsmooth domain which contains domain singularities (such as corners and cracks). The coordinates of the points in $\bar{\Omega}$ will be denoted by (x_1, x_2) as well as (x, y). Let v be a function defined on Ω and define

$$\|v\|^2_{0,\Omega} = \int_\Omega v^2 \, d\Omega; \quad \|v\|^2_{1,\Omega} = \int_\Omega \left[v^2 + \left(\frac{\partial v}{\partial x} \right)^2 + \left(\frac{\partial v}{\partial y} \right)^2 \right] d\Omega.$$

Then, the Hilbert spaces defined by $H^0(\Omega) = \{v : \|v\|_{0,\Omega} < \infty\}$, $H^1(\Omega) = \{v : \|v\|_{1,\Omega} < \infty\}$, are called Sobolev spaces.

Consider a two-dimensional elliptic boundary value problem

$$-\sum_{i,j=1}^{2} \frac{\partial}{\partial x_j} \left(a_{ij}(x) \frac{\partial u}{\partial x_i} \right) = f \quad \text{in } \Omega, \tag{1}$$

$$u = 0 \quad \text{on } \partial\Omega, \tag{2}$$

where $f \in H^0(\Omega)$. Let $H^1_0(\Omega) = \{u \in H^1(\Omega) : u = 0 \text{ on } \partial\Omega\}$. Then the variational equation corresponding to the model problem (1)–(2) is as follows: Find an element $u \in H^1_0(\Omega)$ which satisfies

$$\mathcal{B}(u, v) = \mathcal{F}(v), \quad \text{for any } v \in H^1_0(\Omega), \tag{3}$$

where

$$\mathcal{B}(u, v) = \int_\Omega (\nabla_x v)[a_{ij}](\nabla_x u)^T \, d\Omega, \tag{4}$$

$$\mathcal{F}(v) = \int_\Omega f v \, d\Omega. \tag{5}$$

Here

$$\nabla_x = \left(\frac{\partial}{\partial x_1}, \frac{\partial}{\partial x_2} \right) \equiv \left(\frac{\partial}{\partial x}, \frac{\partial}{\partial y} \right).$$

In the following, $\mathcal{U}(v) = \frac{1}{2}\mathcal{B}(v, v)$ is called the strain energy of v, and $\|v\|_E = \sqrt{\mathcal{U}(v)}$ is called the energy norm of v. By the exact solution of the problem (1)–(2), we mean the unique (weak) solution u_{ex} of the variational equation (3).

2.2. *The Power and the Exponential Auxiliary Mappings*

In this section, we consider two auxiliary mappings which can effectively handle the monotone singularities of the type

$$r^\alpha \quad \text{or } r^\alpha (\log r)^\delta, \tag{6}$$

and the oscillating singularities of the type

$$r^\alpha \cos(\varepsilon \log r), \tag{7}$$

where $0 < \alpha < 1$, and (r, θ) are the polar coordinates of the points in the x-y plane. Here ε is called the **oscillating factor**. It is known that, near a crack front, the displacement functions of homogeneous isotropic materials have the singularities of type (6) [9]. However, for near interfacial cracks of heterogeneous bimaterials, the displacement functions have the oscillating singularities of type (7) [1, 20, 21].

Let $z = x + iy$ and $\zeta = \xi + i\eta$ be complex numbers on the z-plane and the ζ-plane, respectively. By using the conformal mappings $z = \zeta^\beta$ and $z = \exp(\beta\zeta)$ from the ζ-plane onto the z-plane, we define two auxiliary mappings which transform a domain $\hat{\Omega}_S$ in the ξ-η plane onto a neighborhood Ω_S of a singularity (especially, the crack tip) in the x-y plane as follows:

$$\varphi^{\beta}_{pow}(\xi, \eta) = ((\hat{r})^\beta \cos\beta\hat{\theta}, (\hat{r})^\beta \sin\beta\hat{\theta}), \tag{8}$$

and

$$\varphi^{(\beta_1,\beta_2)}_{exp}(\xi, \eta) = (e^{\beta_1\xi} \cos\beta_2\eta, e^{\beta_1\xi} \sin\beta_2\eta), \tag{9}$$

where $(\hat{r}, \hat{\theta})$ denotes the polar coordinates of (ξ, η). The former is called the power auxiliary mapping (PAM) and the later is called the exponential auxiliary mapping (EAM). Here β will be called the mapping size of the auxiliary mappings. We assume that $\beta \geq 1$ for the power auxiliary mapping and β_1 and β_2 can be any positive real numbers for the exponential auxiliary mapping. For brevity, the mapping size vector (β_1, β_2) for EAM will sometimes be denoted by β.

Let $\hat{\Omega}_S$ be the transformed domain of Ω_S by either PAM or EAM. That is, $\hat{\Omega}_S$ denotes either $(\varphi^{\beta}_{pow})^{-1}(\Omega_S)$ or $(\varphi^{\beta}_{exp})^{-1}(\Omega_S)$. Then $\hat{\Omega}_S$ are as shown in Fig. 1 (by PAM) and Fig. 7 (by EAM), respectively.

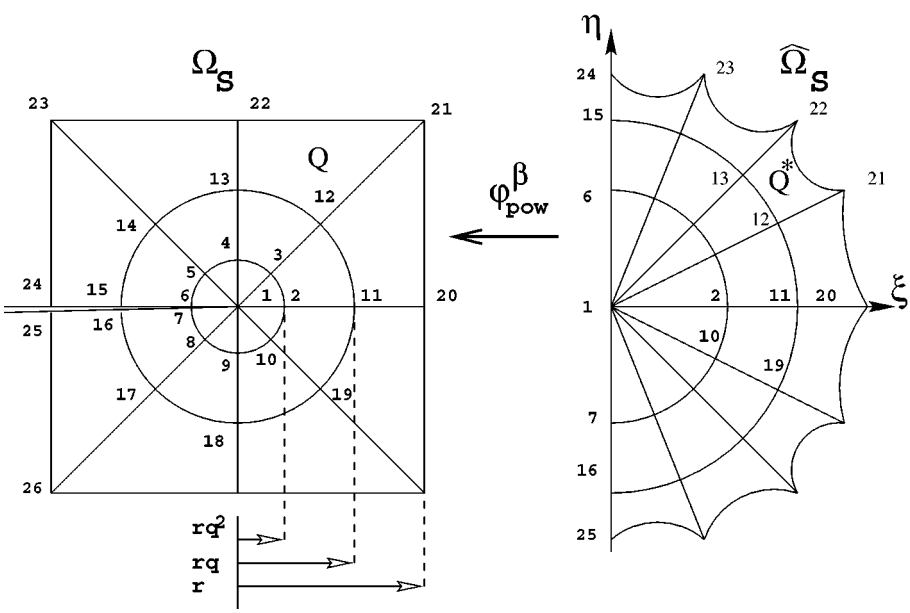

FIG. 1. Scheme of Neighborhood Ω_S of crack tip and the Mapped Neighborhood $\hat{\Omega}_S$ by the power auxiliary mapping φ^{β}_{pow} when $\beta = 2$. The term r should be less than $1/\sqrt{2}$ so that Ω_S can be inside the unit disk.

In what follows, the transformation of a function $u : \Omega_S \to \mathbf{R}$ by the auxiliary mapping φ^{β}_{pow} or φ^{β}_{exp} is denoted by $\hat{u}$. That is, $\hat{u}$ is either $u \circ \varphi^{\beta}_{pow}$ or $u \circ \varphi^{\beta}_{exp}$.

Note that, if a mapping size β of PAM is $1/\alpha$, then $[r^{\alpha}\cos\alpha\theta] \circ \varphi^{\beta}_{pow} = \hat{r}\cos\hat{\theta}$, $[r^{\alpha}(\log r)^{\delta}] \circ \varphi^{\beta}_{pow} = \hat{r}(\beta \log \hat{r})^{\delta}$, and $[r^{\alpha}\cos(\varepsilon \log r)] \circ \varphi^{\beta}_{pow} = \hat{r}\cos(\varepsilon\beta \log \hat{r})$. On the other hand, if a mapping size (β_1, β_2) of EAM is $(\frac{1}{\alpha}, 1)$, then $[r^{\alpha}\cos\alpha\theta] \circ \varphi^{(\beta_1,\beta_2)}_{exp} = e^{\xi}\cos(\alpha\eta)$, $[r^{\alpha}(\log r)^{\delta}] \circ \varphi^{(\beta_1,\beta_2)}_{exp} = e^{\xi}(\xi/\alpha)^{\delta}$, and $[r^{\alpha}\cos(\varepsilon \log r)] \circ \varphi^{(\beta_1,\beta_2)}_{exp} = e^{\xi}\cos(\varepsilon\xi/\alpha)$. Hence, we have the following:

1. By these auxiliary mappings, the intensities of the singularities can be greatly reduced to yield accurate and economical finite element solutions in the framework of the p-version of FEM [7, 8, 23]. In other words, the transformed functions $\hat{u}$ by PAM as well as the transformed functions by EAM, become much smoother than before. Therefore, the polynomial interpolations for these transformed smooth functions defined on $\hat{\Omega}_S$ are improved compared to the polynomial interpolations of the original singular functions defined on Ω_S. PAM is able to remove the power singularity, but the log-singularity and the oscillation still exist. EAM is able to remove the power singularity as well as the log singularity, but the mapped domain $\hat{\Omega}_S$ is infinite (Fig. 7).

2. If $\phi(\xi, \eta)$ is a polynomial on $\hat{\Omega}_S$, then $\phi \circ (\varphi^{\beta}_{pow})^{-1}$ is a singular function on Ω_S, which resembles the corresponding singularity.

3. Furthermore, by the inequality (A.9) and (A.14) in Appendix II, we have the following inequality:

$$\left\|u_{ex} - \phi \circ \left(\varphi^{\beta}_{pow}\right)^{-1}\right\|_{1,\Omega_S} \le \beta \|\hat{u}_{ex} - \phi\|_{1,\hat{\Omega}_S}, \tag{10}$$

$$\left\|u_{ex} - \phi \circ \left(\varphi^{\beta}_{exp}\right)^{-1}\right\|_{1,\Omega_S} \le \beta \|\hat{u}_{ex} - \phi\|_{1,\hat{\Omega}_S,W} \tag{11}$$

Here $\|\cdot\|_{1,\hat{\Omega}_S,W}$ is the weighted norm defined in Appendix II. Since $\hat{u}_{ex}$ becomes a smooth function, it has a good approximation property. For example, if $u_{ex}|_{\Omega_S} = \mathcal{O}(r^{1/4})$, then there is a polynomial $\phi \in \mathcal{P}_p(\hat{\Omega}_S)$ (the set of polynomials on $\hat{\Omega}_S$ of degree $\le p$) such that $\|u_{ex} \circ \varphi^{4}_{pow} - \phi\|_{1,\hat{\Omega}_S} \le Cp^{-2}$ by the arguments with respect to the weighted Besov space ([4]). Hence, by the inequality (10),

$$\left\|u_{ex} - \phi \circ \left(\varphi^{4}_{pow}\right)^{-1}\right\|_{1,\Omega_S} \le 4C/p^2,$$

where p is the degree of basis polynomials. Formal error estimates may be pursued elsewhere by taking advantage of the inequalities (10) and (11), and applying those arguments in [4, 7].

2.3. *The Construction of the Finite Element Spaces by Using PAM and EAM*

Let $\Omega^{(t)}_{st}$ be the standard triangular element in the ξ_t-η_t plane with vertices $V^{(t)}_1 = (-1, 0)$, $V^{(t)}_2 = (1, 0)$, $V^{(t)}_3 = (0, \sqrt{3})$ and $\Omega^{(q)}_{st}$ be the standard quadrilateral element in the ξ_t-η_t plane with vertices $V^{(q)}_1 = (-1, -1)$, $V^{(q)}_2 = (1, -1)$, $V^{(q)}_3 = (1, 1)$, $V^{(q)}_4 = (-1, 1)$.

2.3.1. The construction of singular elemental mapping through φ^{β}_{pow} (Fig. 1). In order to generate a conforming finite element space, special parameterizations for the outer most curved sides are constructed as follows: for example, let $h(\xi_t) : [-1, 1] \to S^{(3)}_Q \subset Q$ be the standard linear mapping, where $S^{(3)}_Q \equiv \overline{21 \to 22}$ is the third side of the quadrilateral element $Q \equiv \overline{13 \to 12 \to 21 \to 22}$ in Ω_S of Fig. 1. Then, in what follows, the parameterization of the curved side $\hat{S}^{(3)}_Q = (\varphi^{\beta}_{pow})^{-1}(S^{(3)}_Q)$, of the curved quadrilateral element

$Q^* = (\varphi_{pow}^{\beta})^{-1}(Q)$ in $\hat{\Omega}_S$, is defined by

$$(\xi(\xi_t), \eta(\xi_t)) = \left[\left(\varphi_{pow}^{\beta}\right)^{-1} \circ h\right](\xi_t). \tag{12}$$

Let Ψ_Q^* be a blending type elemental mapping from $\Omega_{st}^{(q)}$ onto a curved quadrilateral element Q^* obtained by using the parameterization (12) for the curved side $\hat{S}_Q^{(3)}$ and the standard parameterization for the circular curve side $(\varphi_{pow}^{\beta})^{-1}(\overline{13 \to 12})$ (see Chapter 6 of [23]). Then the a Singular Elemental Mapping from $\Omega_{st}^{(q)}$ onto Q is defined by

$$\Psi_Q^S(\xi_t, \eta_t) = \left[\varphi_{pow}^{\beta} \circ \Psi_Q^*\right](\xi_t, \eta_t).$$

Then for a standard shape function ϕ on $\Omega_{st}^{(q)}$, $\phi \circ (\Psi_Q^S)^{-1}$ is a singular shape function on Q, which resembles a $r^{1/\beta}$-type singular function. The singular elemental mappings from $\Omega_{st}^{(t)}$ to curved triangular elements with one curved side in $\hat{\Omega}_S$ are constructed in a similar manner.

Now for the eight triangular elements with one curved side and 16 quadrilateral elements with two curved sides, we construct singular elemental mappings as follows: for $1 \le k \le 8$,

$$\Psi_k^S = \varphi_{pow}^{\beta} \circ \Psi_k^* : \Omega_{st}^{(t)} \to T_k \equiv \varphi_{pow}^{\beta}(T_k^*) \tag{13}$$

and for $9 \le k \le 24$,

$$\Psi_k^S = \varphi_{pow}^{\beta} \circ \Psi_k^* : \Omega_{st}^{(q)} \to Q_k \equiv \varphi_{pow}^{\beta}(Q_k^*). \tag{14}$$

Let us note that by the particular construction of the parameterization (12), $\Psi_Q^S(\xi_t, 1) = \Psi_Q(\xi_t, 1)$ is linear in ξ_t, where Ψ_Q is the conventional elemental mapping from $\Omega_{st}^{(t)}$ onto Q. Hence, the singular elemental mappings $\Psi_{17}^S, \ldots, \Psi_{24}^S$ agree with the conventional elemental mappings $\Psi_{25}, \ldots, \Psi_{32}$ along the common sides between Q_{17} and E_{25}, Q_{18} and E_{26}, and so on. Here $E_{25}, \ldots, E_{24}$ are elements in $\Omega \backslash \Omega_S$ which share one straight side with quadrilateral elements $Q_{17}, \ldots, Q_{24}$, respectively (see Fig. 1). Thus, the finite element space constructed through these elemental mappings is **"exactly conforming"** [23]. In other words, each member of the finite element space constructed below is continuous in order to ensure good approximation properties.

2.3.2. The construction of singular elemental mapping through φ_{exp}^{β} (Fig. 7). The singular elemental mappings Ψ_k^S through the exponential auxiliary mapping φ_{exp}^{β} are constructed in Appendix III.

2.3.3. Construction of Finite Element Space. Suppose $\Delta = \{E_k : k = 1, 2, \ldots, N(\Delta)\}$ represents a specific mesh on Ω such that the neighborhoods $\Omega_S \subset \Omega$ of the singularities are partitioned as shown in either Fig. 1 or Fig. 7. Let $\mathcal{M}$ be the vector of elemental mappings assigned to the elements in Δ by the following rule:

1. Assign the conventional elemental mappings to the elements in $\Omega \backslash \Omega_S$;
2. Assign the singular elemental mappings defined by 13 and 14 to the elements in Ω_S.

Suppose $\Omega_{st}^{(*)}$ represents either the standard triangular element or the standard quadrilateral element and $\mathcal{P}_p(\Omega_{st}^{(*)})$ is the space of polynomials of degree p defined on $\Omega_{st}^{(*)}$. Then the finite element space, denoted by $S^p(\Omega, \Delta, \mathcal{M})$, is the set of all functions u defined on Ω such that

1. The strain energy of u is finite,
2. $u \circ \Psi_k^S \in \mathcal{P}_p(\Omega_{st}^{(t)})$ if $k \leq 8$ and $u \circ \Psi_k^S \in \mathcal{P}_p(\Omega_{st}^{(q)})$ if $9 \leq k \leq 24$,
3. $u \circ \Psi_k \in \mathcal{P}_p(\Omega_{st}^{(*)})$ for the elements in $\Omega \backslash \Omega_S$.

Now, the finite element solution u_{fe} is the projection of the exact solution onto $S^p(\Omega, \Delta, \mathcal{M})$. The dimension of the vector space $S^p(\Omega, \Delta, \mathcal{M})$ is called the Number of Degree of Freedom.

In the p-version of the finite element method [3, 7, 8, 23], to obtain the desired accuracy, the mesh Δ of the domain is fixed and only the degree p of the basis polynomials is increased.

Additional work may be required to construct the singular basis functions of the finite element space $S^p(\Omega, \Delta, \mathcal{M})$, (which were constructed through PAM or EAM), for the computations of the local stiffness matrices and local load vectors. The novelty of this method is this additional work may be avoided by the following:

• Instead of constructing the singular basis functions of $S^p(\Omega, \Delta, \mathcal{M})$ for the local stiffness matrices and the local load vectors for the elements (denoted by E_k which stands for either a triangular element T_k or a quadrilateral element Q_k) in Ω_S, we use either the transformed bilinear form $\mathcal{B}^*(\cdot, \cdot)$ and the transformed linear functional $\mathcal{F}^*(\cdot)$, defined in Lemma AI.2 or $\hat{\mathcal{B}}(\cdot, \cdot)$ and $\hat{\mathcal{F}}(\cdot)$, defined in Lemma AI.1.

In other words, for the local stiffness matrices and local load vectors of the elements $E_k \subset \Omega_S$, we use the conventional FEM to compute local stiffness matrices and local load vectors of the corresponding mapped elements E_k^* in $\hat{\Omega}_S$ (if PAM is used) and $\hat{E}_k$ in $\hat{\Omega}_S$ (if EAM is used), respectively.

Thus, the proposed method requires virtually no more extra work than the conventional FEM. In other words, the only extra work involved for this method is that in order to calculate the local stiffness matrices and the local load vectors of elements in Ω_S, the transformed bilinear form (either $\mathcal{B}^*(\cdot, \cdot)$ or $\hat{\mathcal{B}}(\cdot, \cdot)$), and the transformed linear functional (either $\mathcal{F}^*(\cdot)$ or $\hat{\mathcal{F}}(\cdot)$) will be used, instead of the original bilinear form and the original linear functional. Let us note the original bilinear form and the linear functional are the left side integrals in Appendix I. Of course, the bilinear form for the local stiffness matrices and the linear functional for local load vectors of those elements in $\Omega \backslash \Omega_S$ are, respectively, the original bilinear form $\mathcal{B}(\cdot, \cdot)$ and the original linear functional $\mathcal{F}(\cdot)$.

3. NUMERICAL RESULTS

This section demonstrates the effectiveness of the power auxiliary mapping as well as the exponential auxiliary mapping in dealing with singularities.

For a clear presentation of the effectiveness of mapping techniques, we consider the Poisson equation,

$$-\Delta u = f \quad \text{on} \quad \Omega = \{(r, \theta) : r \leq r_0,\ 0 \leq \theta \leq \pi\},$$

(see Fig. 2) for which the exact solution is one of the following hypothetical singular functions:

1. $u_1(r, \theta) = (r^{0.5} + 0.05r^5) \cos\theta$,
2. $u_2(r, \theta) = r^{0.25}(\log r)^2 \cos\theta$ (or $r^{0.5}(\log r)^2 \cos\theta$),
3. $u_3(r, \theta) = r^{0.5}(\sin(0.1 \cdot \log r)) \cos\theta$,
4. $u_4(r, \theta) = r^{0.5}(\sin(3 \log r)) \cos\theta$.

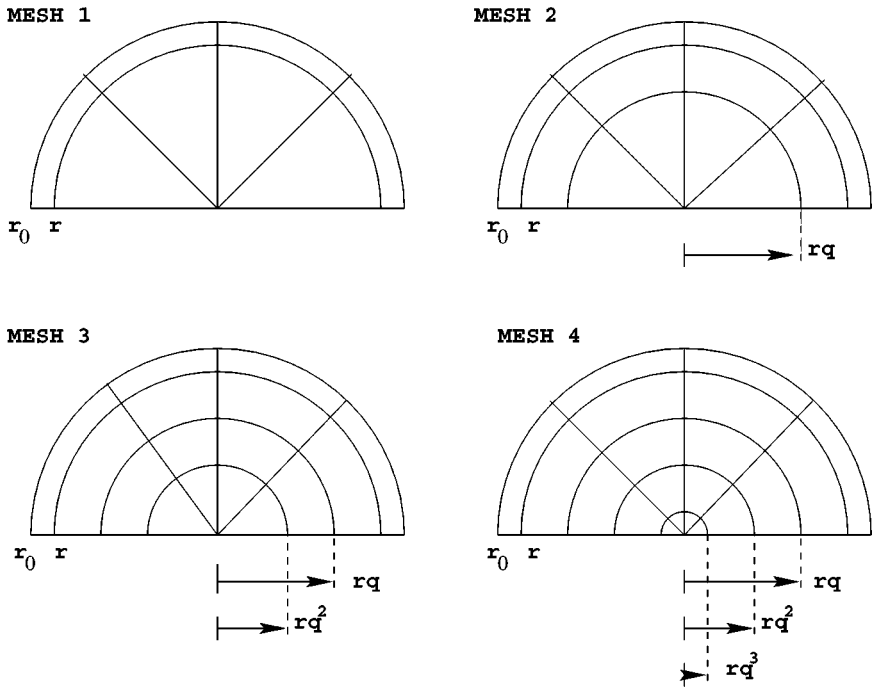

FIG. 2. Scheme of the domain of the test problems and various geometric mesh refinements with respect to the ratio q.

In all of the numerical examples of this section, traction boundary conditions are imposed along the boundary, and the origin is fixed. The p-distribution for the p-version of FEM is restricted to be uniform (that is, in the construction of elemental shape functions, the degree of the basis polynomials of the master element takes the value p for all elements).

It is known (18, 23) that $\|u_{fe} - u_{ex}\|_E^2 = |\mathcal{U}(u_{fe}) - \mathcal{U}(u_{ex})|$, provided that all boundary conditions are either homogeneous Dirichlet or arbitrary traction boundary conditions. In this section, by the Relative Error (%) in Energy Norm, we mean

$$100 \cdot \left[\frac{|\mathcal{U}(u_{ex}) - \mathcal{U}(u_{fe})|}{\mathcal{U}(u_{ex})} \right]^{1/2}. \tag{15}$$

First, suppose an asymptotic expansion of the solution of an elliptic equation at a singularity point (caused by the irregularity of a solution domain) has the form ([22])

$$u(r, \theta) = \sum_{n=1}^{N} c_n r^{\lambda n} f_n(\theta) + v(r, \theta), \tag{16}$$

where $v \in H^2(\Omega)$, which is the collection of all measurable functions v such that $\int_\Omega [v^2 + \nabla v \cdot \nabla v + (\frac{\partial^2 v}{\partial x^2})^2 + (\frac{\partial^2 v}{\partial x \partial y})^2 + (\frac{\partial^2 v}{\partial y^2})^2] dx dy < \infty$. In most practical problems of fracture mechanics, the smoother terms v have little influence on the solution at the points close to the singularity point. Thus, in this paper, *the assumption is that the coefficients of higher order terms of the asymptotic expansion of solutions at singularity points are zero (that is, $v = 0$ in (16)).*

However, if the coefficients of some higher order terms are not negligible, then care must be exercised in applying this method. For example, suppose v contains a term of the form $c_m r^{10} f_m(\theta)$ and c_m is large, then $[c_m r^{10} f_m(\theta)] \circ \varphi^4_{pow} = c_m(\hat{r})^{40} \hat{f}_m(\hat{\theta})$ cannot have good approximation properties on the mapped singular region $\hat{\Omega}_S$ in case the diameter of $\hat{\Omega}_S$ is >1, unless the degree of basis polynomials are very large. However, if a neighborhood Ω_S of a singularity point is chosen to be small, for example $\Omega_S = \Omega \cap \{(r, \theta) : r \leq 0.15\}$, then we have $\hat{\Omega}_S \subset \{(\hat{r}, \hat{\theta}) : \hat{r} \leq 0.63\}$, on which $(\hat{r})^{40}$ is almost zero.

The first example demonstrates the justification of the forgoing arguments.

EXAMPLE 3.1. r^α type singular function plus higher order terms. We assume that the domain for this case is the upper half unit disk $\Omega = \{(r, \theta) : 0 \leq \theta \leq \pi, r \leq 1\}$. Then, the strain energy is

$$\mathcal{U}(u_1) = \frac{1}{2} \int_\Omega \nabla u_1 \cdot \nabla u_1 = 1.036832676,$$

and $-\Delta u_1 = 0.15(\cos\theta)(5r^2 - 8r^{13/2})/r^{7/2}$.

If we select $\beta = 4$ for the mapping size of the power auxiliary mapping, and the neighborhood of the singularity point is $\Omega_S = \{(r, \theta) : r \leq 0.15, 0 \leq \theta \leq \pi\}$, then on the mapped domain $\hat{\Omega}_S$, the first term, $\hat{r}^2 \cos 4\hat{\theta}$, of the mapped solution $\hat{u}_1 = u_1 \circ \varphi^4_{pow}$, is the dominating term and the high-order second term, $0.05(\hat{r})^{20} \cos 4\hat{\theta}$, of $\hat{u}_1$, is almost zero. Therefore, the additional high-order term does not deter for MAM to yield a highly accurate finite element solution as shown in Fig. 3. The geometric ratio $q = 0.15$ is used for the mesh for the finite element analysis in Fig. 3.

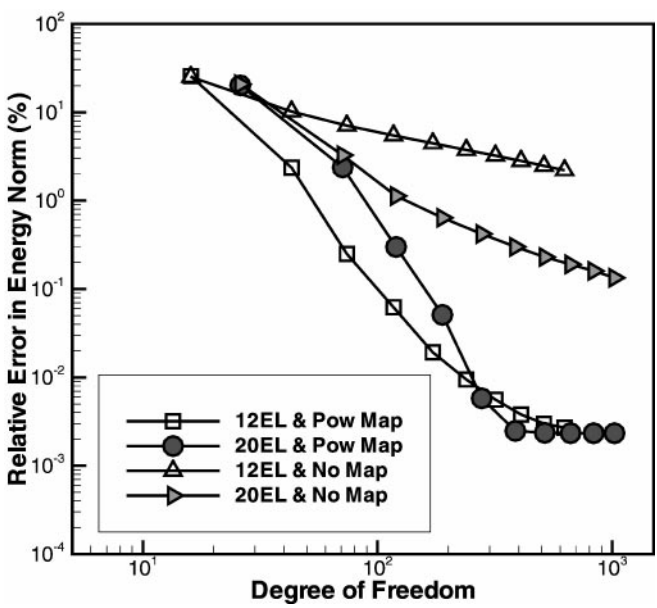

FIG. 3. The relative errors (%) in Energy Norm when the solution is $u_1(r, \theta) = (r^{0.25} + 0.05r^5)\cos\theta$, which contains the r^α type singularity. "Pow Map" indicates the results obtained by the power auxiliary mapping φ^β_{pow} with $\beta = 4$.

In Fig. 3, the relative errors of FE solutions obtained by the power auxiliary mapping (PAM) with mapping size 4 and those obtained without using the mapping techniques, respectively, are 0.0038% and 2.82%, when p-degree is 8 and the discretization of Ω is a coarse mesh of 12 elements (which is Mesh 2 of Fig. 2) when the radii are 1, 0.5, 0.15.

For the numerical results in Fig. 3, $\Omega_S = \{(r, \theta) : 0 \le \theta \le \pi, r \le 0.5\}$ is used for a neighborhood of the singularity and hence the regular region is $\Omega_R = \{(r, \theta) : 0.5 < \theta < 1\}$. However, the corresponding results obtained by selecting a smaller neighborhood $\Omega_S = \{(r, \theta) : |r| \le 0.15\} \cap \Omega$ of the singularity are similar to those in Fig. 3.

Because of the nature of PAM, in dealing with r^α type singularity, MAM does not need a massive mesh refinement. Rather, the results obtained by applying MAM on the 12-element mesh are almost the same as those obtained by applying MAM on the 20-element mesh (which is Mesh 4 of Fig. 2 when the radii are $1, 0.5, 0.15, 0.15^2, 0.15^3$). For example, when the p-degree is 8, the relative errors are 0.0038% for the 12-element coarse mesh and 0.0024% for the geometric refined mesh of 20 elements.

Furthermore, the results in Fig. 3 demonstrate MAM superiority over the conventional p-version of FEM in dealing with r^α type monotone singularity.

For the h-p version of FEM, the diagram of the geometric meshes are listed in Fig. 2 as follows:

a: Mesh 1 represents the basic mesh by two co-centered circles of radii r_0, r with no layers around the singularity point.

b: Mesh 2 represents the geometrically refined mesh obtained by placing one layer of radius rq.

c: Mesh 3 and Mesh 4 are the geometrically refined meshes by placing two layers of radius rq, rq^2, and by placing three layers of radii rq, rq^2, rq^3, respectively.

d: Similarly, Mesh 8 is the geometrically refined mesh by placing seven layers of radii $rq, rq^2, rq^3, rq^4, rq^5, rq^6, rq^7$.

The h-p version of FEM is the combination of refining mesh and increasing degree of basis functions as follows: Mesh 1 and p-degree $= 1$, Mesh 2 and p-degree $= 2$, Mesh 3 and p-degree $= 3$, Mesh 4 and p-degree $= 4$, and so on.

In the second example, to demonstrate the effectiveness of MAM in dealing with the $\log^\delta r$-type singularity, MAM is compared with the h-p method.

EXAMPLE 3.2. $r^\alpha \log^\delta r$-type singular function. The domain for this case is the upper half disk (Fig. 2) where the radius of the outer circle is 2. Then the strain energy of $u_2 = r^{0.25} \log^2 r \cos\theta$ is

$$\mathcal{U}(u_2) = \frac{1}{2} \int_\Omega \nabla u_2 \cdot \nabla u_2 = 616.3010106,$$

and $-\Delta u_2 = 0.0625(\cos\theta)(15 \log^2 r - 16 \log r - 32)/r^{7/4}$.

In this example, $\Omega_S = \{(r, \theta) : r \le 1, 0 \le \theta \le \pi\}$ is used for the neighborhood of the singularity point. In dealing with this type of singularity,

1. If PAM φ^4_{pow} is used, then $u_2 \circ \varphi^4_{pow} = 16\hat{r} \log^2 \hat{r} \cos\hat{\theta}$, which becomes smoother than u_2. However, the log-singularity is still there.

2. If EAM $\varphi_{exp}^{(4,1)}$ is used, then $u_2 \circ \varphi_{exp}^{(4,1)} = 16e^{\xi}\xi^2 \cos\eta$, which becomes a smooth function on the infinite strip $(-\infty, 0] \times [-\pi, \pi]$ on the ξ-η plane.

Now the results obtained by MAM with respect to PAM and EAM are compared with the results obtained by the h-p method with mesh refinement by the geometric ratio $q = 0.15$ and the h-p method with mesh refinement by the geometric ratio $q = e^{-1.5\pi}$ in Table I.

In Table I, "POW ($\beta = 4$)" represents the results obtained by applying MAM with respect to PAM of the mapping size 4 on Mesh 5 obtained by the ratio $q = (0.15)^4$. "EXP ($\beta = (4, 1)$)" represents the results obtained by applying MAM with respect to EAM of the mapping size $(4, 1)$ on Mesh 5 obtained by the ratio $q = e^{-2\pi}$. From this example, the following facts are observed:

1. Table I demonstrates that EAM with mapping size (4, 1) yields the best economic FE solutions among the three methods: the h-p method, PAM, and EAM. Since, for EAM, Mesh 5 is constructed by the ratio $q = e^{-2\pi}$, under the mapping $\varphi_{exp}^{(4,1)}$, the mapped mesh on $\hat{\Omega}_S = (-\infty, 0] \times [-\pi, \pi]$ becomes a uniform mesh such that $(-\infty, 0]$ is divided into $(-\infty, -8\pi/4]$, $[-8\pi/4, -6\pi/4]$, $[-6\pi/4, -4\pi/4]$, $[-4\pi/4, -2\pi/4]$, and $[-2\pi/4, 0]$ (Fig. 7).

On the other hand, the mapped true solution $\hat{u}_2$ by PAM φ_{pow}^4 does not have $\hat{r}^{\alpha}$-type singularity. However, $\hat{u}_2$ still has $\log^2 \hat{r}$-type singularity. To handle the remaining singularity, $\log^2 \hat{r}$, the mapped domain $\hat{\Omega}_S$ is geometrically refined by the ratio $q = 0.15$.

TABLE I

The Relative Error (%) in Energy Norm When $u_2 = r^{0.25} \log^2 r \cos\theta$ Is the True Solution and When $u_2 = r^{0.5} \log^2 r \cos\theta$ Is the True Solution

The h-p Method with ratio q				The Mapping Method with map size β		
p-deg	DOF	$q = 0.15$	$q = e^{-1.5\pi}$	DOF	POW ($\beta = 4$)	EXP ($\beta = (4, 1)$)
			$r^{0.25}(\log^2 r)\cos\theta$			
1	11	99.96	99.96	31	25.27	24.37
2	43	97.65	87.43	85	5.817	5.560
3	97	87.67	53.38	143	2.742	1.782
4	189	73.08	28.06	225	1.160	0.549
5	331	57.80	15.93	331	0.563	0.313
6	535	44.05	11.91	461	0.431	0.149
7	813	32.65	10.88	615	0.396	0.103
8	1177	23.70		793	0.382	0.028
			$\sqrt{r}(\log^2 r)\cos\theta$			
1	11	98.38		31	25.14	45.49
2	43	78.33	42.85	85	5.235	9.025
3	97	44.16	14.39	143	1.445	6.977
4	189	21.80	10.82	225	0.517	1.869
5	331	10.09	9.96	331	0.236	0.538
6	535	4.50	9.40	461	0.130	0.148
7	813	1.95	9.00	615	0.078	0.033
8	1177			793	0.050	0.005

For this purpose, Ω_S is refined by the ratio $q = 0.15^4$. Then the mapped mesh on the mapped domain $\hat{\Omega}_S$ becomes a geometrically refined mesh by the ratio $q = 0.15$.

2. For the geometric mesh refinement of the conventional p-version of FEM, the ratio $q = e^{-1.5\pi}$ yields better results than the ratio $q = 0.15$ which is an optimal geometric ratio to deal with the r^α-type monotone singularity [23]. Actually, of the ratios $q = 0.15, q = e^{-\pi}, q = e^{-1.5\pi}, q = e^{-2\pi}$, the ratio $q = e^{-1.5\pi}$ yields the best results. However, as we can see on the bottom half of Table I, the h-p method with respect to mesh refinement by $q = 0.15$ converges faster than the h-p method with respect to mesh refinement by $q = e^{-1.5\pi}$ when the intensity of singularity is the same as the crack singularity.

3. The results of Table I are depicted in Fig. 4 on the log-log scale. Fig. 4 shows that MAM (with PAM or EAM) yields better results than the h-p method with either geometric ratio $q = e^{-1.5\pi}$ or $q = 0.15$. If $q = e^{-1.5\pi}$ is used for the geometric mesh for the conventional p-version of FEM, the results by Mesh 7 are not better than the results by Mesh 6 because q^6 is already too small. Thus, "h-p with $q = e^{-1.5\pi}$" on Table I stopped when the p-degree reached seven. In most practical computations by the h-p method, the refining mesh usually stops at Mesh 6.

Let us note that in dealing with $r^\alpha \log^\delta r$ type singularity, EAM performs better than PAM. The above mesh refinement for EAM may not be optimal. An optimal mesh for EAM is under investigation.

In the next two examples, we consider a function which contains the oscillating singularity of type $r^\alpha \sin(\varepsilon \log r)$ with respect to various sizes ε of oscillating factor.

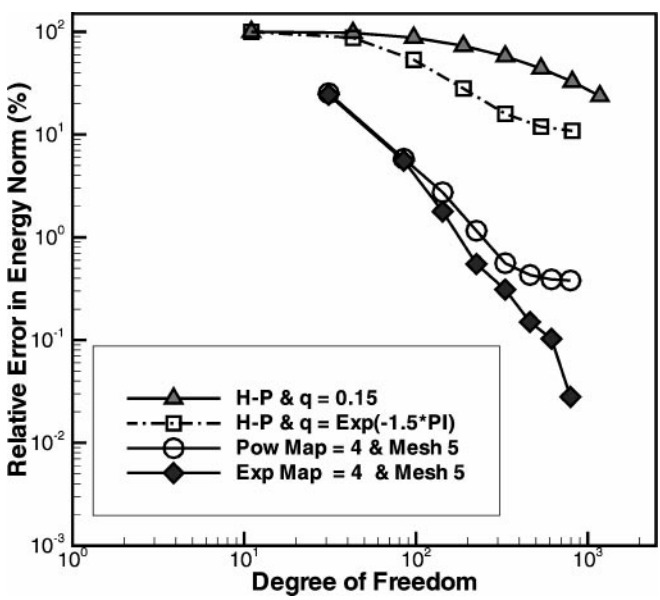

FIG. 4. The relative errors (%) in Energy Norm when the solution is $u_2(r, \theta) = r^{0.25}(\log^2 r)\cos\theta$, which contains the $r^\alpha \log^\delta r$ type singularity. "H-P & $q = 0.15$ " and "H-P & $q = e^{-1.5\pi}$" stand for the results obtained by the h-p method with respect to the ratios $q = 0.15$ and $q = e^{-1.5\pi}$, respectively.

EXAMPLE 3.3. Weakly oscillating singular functions with small oscillating factor ($\varepsilon \leq 0.17$). The domain for this example is the upper half disk (Fig. 2) with radius 2. The strain energy is

$$\mathcal{U}(u_3) = \frac{1}{2}\int_\Omega \nabla u_3 \cdot \nabla u_3 = 0.03174559397,$$

and $-\Delta u_1 = 0.15(\cos t)(5r^2 - 8r^{13/2})/r^{7/2}$.

By PAM φ^4_{pow}, the oscillating singular function is transformed to $\hat{u}_3 = u_3 \circ \varphi^4_{pow} = \hat{r}^2 \sin(0.4 \log \hat{r}) \cos\hat{\theta}$ on $\hat{\Omega}_S$ which contains no more $\hat{r}^\alpha$-type singularity, but has a small oscillating factor. Thus, it is not necessary to refine the mapped domain $\hat{\Omega}_S$ for a large improvement. That is, MAM yields improved results at low cost (small DOF). However, if the oscillating factor were $\varepsilon \geq 1$, then $\hat{u}_3$ could have been highly oscillating (see, Example 3.4). In Table II, "Mesh 2 & Map = 4," and "Mesh 4 & Map = 4," respectively, indicate the results obtained by MAM with mapping size 4 on Mesh 2 (the geometrically refined mesh of Mesh 1 obtained by putting one layer) and by MAM with mapping size 4 on Mesh 4 (the mesh obtained by putting three layers in Mesh 1). Here the ratio for mesh refinement is $q = 0.15$. On the other hand,"Mesh 2 & No Map" indicates the results obtained by the conventional p-method without using mapping techniques.

From this example, we have the following conclusions:

1. Unlike the results in Example 3.2, the geometric ratio $q = 0.15$ for the p-version of FEM yields the best results among the four ratios: $q = 0.15$, $q = e^{-\pi}$, $q = e^{-1.5\pi}$, and $q = e^{-2\pi}$.

2. The numerical results in Table II are depicted in Fig. 5, which demonstrates MAM with respect to PAM yields better results than the conventional p-version of FEM.

3. If the oscillating factor were $\varepsilon = 3$ (Example 3.4), the oscillating factor of the mapped function by φ^4_{pow} is 12, which means the mapped function is highly oscillating on the mapped domain $\hat{\Omega}_S$. Thus, MAM alone cannot yield much improved results. However, if the oscillating factor $\varepsilon \leq 0.17$, the mapped true solution $\hat{u}_3$ by φ^4_{pow} is still weakly oscillating and hence the MAM with respect to PAM could yield the much improved results as shown in Table II.

TABLE II
The Relative Errors (%) in Energy Norm When the True Solution Is $u_3 = r^{0.5}\sin(0.1 \cdot \log r)\cos\theta$

p-deg	DOF	Mesh 2 & No Map	Mesh 2 & Map = 4	DOF	Mesh 2 & No Map	Mesh 2 & Map = 4
1	21	28.83	25.133	26	20.80	24.005
2	57	16.42	4.6964	71	0.717	2.3628
3	97	12.17	1.4780	120	4.183	1.2987
4	153	9.761	0.2361	189	2.709	0.1465
5	225	8.185	0.0668	278	1.942	0.0133
6	313	7.049	0.0275	387	1.500	0.0034
7	417	6.181	0.0139	516	1.217	0.0015
8	537	5.487	0.0086	665	1.021	0.0010
9	673	4.913	0.0063	834	0.877	0.0016

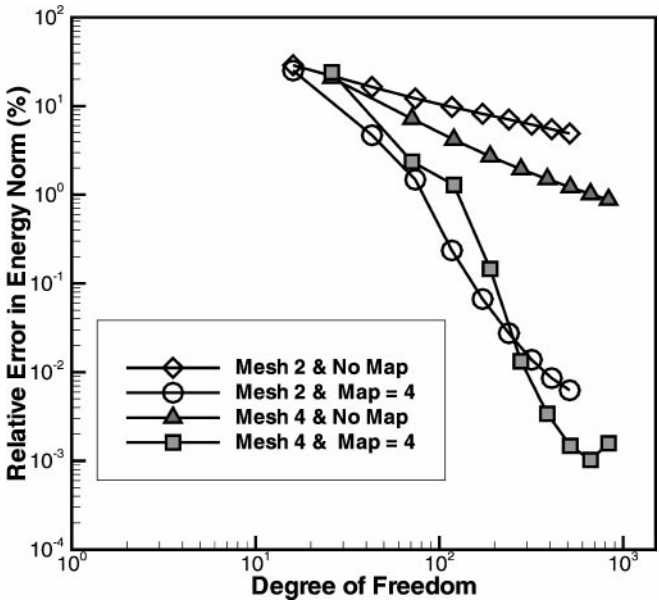

FIG. 5. The relative errors (%) in Energy Norm when the solution is $u_3(r,\theta) = r^{0.5}\sin(0.1 \cdot \log r)\cos\theta$, which contains an oscillating singularity.

As the oscillating factor becomes smaller, the singularity function is less oscillating. As one can see from Fig. 5, MAM gives highly accurate solutions at low cost when the oscillating factor ε is small. In most practical problems of fracture mechanics, ε is small. Actually, it is known [16] that the maximum value of the oscillating factors for the interfacial cracks of bimaterials is $\varepsilon = 0.17$.

Finally, we consider a problem which contains a highly oscillating singularity.

EXAMPLE 3.4. Highly oscillating singular functions with large oscillating factor ($\varepsilon > 1$). The domain for this example is the upper half disk of radius 2 in Fig. 2, and the neighborhood of the singularity point is $\Omega_S = \{(r,\theta) : 0 \le \theta \le \pi, r \le 1\}$. Then the strain energy is

$$\mathcal{U}(u_4) = \frac{1}{2}\int_\Omega \nabla u_4 \cdot \nabla u_4 = 7.270858618,$$

and $-\Delta u_4 = 0.75(\cos t)(-13\sin(3\log r) + 4\cos(3\log r))/r^{3/2}$.

By PAM φ^4_{pow}, u_4 is transformed to $\hat{u}_4 = \hat{r}^2\sin(12 \cdot \log\hat{r})\cos(\hat{\theta})$ which has a large oscillating factor ($\varepsilon = 12$). Thus, $\hat{u}_4$ still has poor approximation properties even though the singularity of type r^α disappeared.

In order to make the oscillating factor as small as possible while maintaining a good mapping effect in dealing with the r^α-singularity, we use PAM with mapping size $\beta = 2$.

In this paper, the local stiffness matrices and local load vectors are computed by the Gaussian quadrature formula of 12×12 gauss points for every level of p-degree. However, because of the large oscillating factor ($\varepsilon = 6$), the errors of the numerical integrals of the local load vector $\int_{\hat{E}} |J(\varphi^2_{pow})|(-\Delta u_4) \circ (\varphi^2_{pow})\hat{\phi}\, d\xi\, d\eta$ are not small, whenever E is a triangular element containing this singularity point. Thus, MAM is not able to give a large improvement.

TABLE III
The Relative Errors (%) in Energy Norm When the True Solution Is $u_4 = r^{0.5}\sin(3 \cdot \log r)\cos\theta$

p-deg	DOF	h-p & $q = 0.15$	DOF	Mesh 8 & No Map	Mesh 8 & Map = 2
1	11	88.22	45	88.05	88.35
2	42	45.80	126	42.96	54.54
3	96	39.51	211	38.81	29.00
4	188	18.68	332	18.52	7.41
5	330	5.67	489	5.61	5.11
6	534	2.08	682	2.07	1.41
7	812	1.54	911	1.53	0.24
8	1176	0.96	1176	0.96	0.09

From this example, we have observed the following facts:

1. The numerical results in Table III are depicted in Fig. 6, which demonstrates MAM with respect to PAM yields better results than the h-p method with respect to mesh refinement by $q = 0.15$.

2. The mapped function is highly oscillating on the mapped domain $\hat{\Omega}_S$ since the oscillating factor of the mapped function by φ^2_{pow} is 6. Thus, MAM alone cannot yield much improved results. If larger numbers of Gauss points, in computations of the local load vectors for the elements containing the singular point, were used, MAM on Mesh 8 could have yielded more accurate solutions.

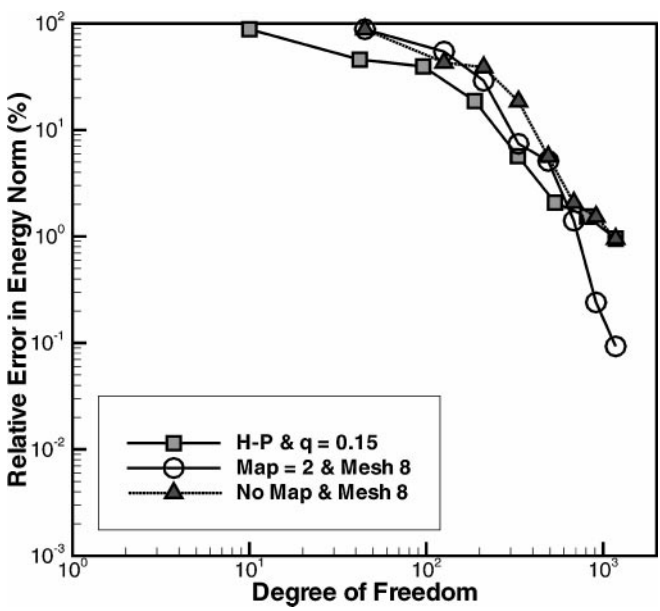

FIG. 6. The relative errors (%) in Energy Norm when the solution is $u_4(r, \theta) = r^{0.5}\sin(3 \cdot \log r)\cos\theta$, which contains highly oscillating singularity ($\epsilon = 3$).

3. MAM with respect to EAM yields as good results as those in Table III. However, much improved results are expected by employing EAM whenever the treatments for infinite elements are selected in an optimal manner.

4. CONCLUDING REMARKS

EAM is more advantageous than PAM when the intensity α in the $r^\alpha, r^\alpha \log^\delta r, r^\alpha \sin(\varepsilon \log r)$ types of singularity is not known in advance. However, its drawback is that the mapped neighborhood $\hat{\Omega}_S$ of a singularity point becomes an infinite strip, and hence infinite elements should be introduced. In this paper, a preliminary report on EAM is presented. Extensive research on EAM (including shape functions for infinite elements, optimal meshes on the infinite strip, and so on) should be done. Since EAM yields the best economical FE solutions for the problems containing $r^\alpha \log^\delta r$-type singularity, EAM is promising in dealing with oscillating singularities.

The r^α-singularity and the log-term of the oscillating singularity of the type $r^\alpha \sin(\varepsilon \log r)$ can be destroyed by EAM $\varphi_{exp}^{(\beta_1,\beta_2)}$. However, if $\beta_1 \geq 1$, then the sine function is more oscillating. Thus, the shape functions on the singular region Ω_S generated by the infinite elements and EAM (described in Appendix III) may not be optimal in dealing with the oscillating singularity.

For the problems containing the singularity of types r^α or $r^\alpha \sin(\varepsilon \log r)$ with small $\varepsilon(\ll 1)$, PAM is very effective. Thus, for such cases, introduction of EAM is not necessary.

The numerical tests demonstrate MAM with respect to EAM as well as MAM with respect to PAM yield better economical FE solutions for the problems containing singularities than the h-p version of FEM and the conventional p-version of FEM whenever intensity of singularity and type of singularity is known in advance.

Finally, let us comment on the applications and the 3D extensions of the mapping methods. The methods developed in this paper were applied to composite materials [16] to obtain highly accurate energy release rates for delamination cracks in laminated plates. There are three different types of 3D singularities: the vertex, the edge and the vertex-edge combined singularities [20, 21]. At the tip of a crack in heterogeneous materials, these singularities are oscillating. The methods of this paper can easily be extended so that it can handle the oscillating edge singularities arising in composite materials. However, the behavior of the oscillating vertex-edge singularities is different from the 2D counterpart. Preliminary work for 3D extension of PAM for monotone singularities can be found in [13].

APPENDIX I

The Transformed Principal of Virtual Work by the Auxiliary Mappings

The determinants of the Jacobian matrices of the power auxiliary mapping φ_{pow}^{β} and the exponential auxiliary mapping $\varphi_{exp}^{(\beta_1,\beta_2)}$ are

$$\left|J\left(\varphi_{pow}^{\beta}\right)\right| = \beta^2(\hat{r})^{2(\beta-1)} \quad \text{and} \quad \left|J\left(\varphi_{exp}^{\beta}\right)\right| = \beta_1\beta_2 e^{2\beta_1\xi}, \tag{A.1}$$

respectively.

Let $\nabla_x = (\frac{\partial}{\partial x}, \frac{\partial}{\partial y})$ and $\nabla_\xi = (\frac{\partial}{\partial \xi}, \frac{\partial}{\partial \eta})$. In what follows, we will obtain the transformed bilinear forms and the transformed linear functionals corresponding to the two auxiliary mappings.

LEMMA AI.1. *Let $u, v \in H^1(\Omega_S)$, then by the exponential auxiliary mapping $\varphi_{exp}^{(\beta_1,\beta_2)}$, the bilinear form* (4) *and the linear functional* (5)*, are transformed to the forms*

$$\begin{aligned}\mathcal{B}(u,v) &\equiv \int_{\Omega_S} (\nabla_x u)\begin{bmatrix} a_{11} & a_{12} \\ a_{21} & a_{22}\end{bmatrix}(\nabla_x v)^T\,dx\,dy \\ &= \int_{\hat{\Omega}_S} (\nabla_\xi \hat{u})\begin{bmatrix} c_{11} & c_{12} \\ c_{21} & c_{22}\end{bmatrix}(\nabla_\xi \hat{v})^T d\xi\,d\eta \equiv \hat{\mathcal{B}}(\hat{u},\hat{v}),\end{aligned} \tag{A.2}$$

where

$$\begin{aligned}c_{11} &= \frac{\beta_2}{\beta_1}[a_{11}\cos^2(\beta_2\eta) + (a_{21}+a_{12})\cos(\beta_2\eta)\sin(\beta_2\eta) + a_{22}\sin^2(\beta_2\eta)], \\ c_{12} &= (a_{22}-a_{11})\sin(\beta_2\eta)\cos(\beta_2\eta) - a_{21}\sin^2(\beta_2\eta) + a_{12}\cos^2(\beta_2\eta), \\ c_{21} &= (a_{22}-a_{11})\sin(\beta_2\eta)\cos(\beta_2\eta) + a_{21}\cos^2(\beta_2\eta) - a_{12}\sin^2(\beta_2\eta), \\ c_{22} &= \frac{\beta_1}{\beta_2}[a_{11}\sin^2(\beta_2\eta) - (a_{12}+a_{21})\sin(\beta_2\eta)\cos^2(\beta_2\eta) + a_{22}\cos^2(\beta_2\eta)].\end{aligned}$$

For $v \in H^1(\Omega_S)$ and $f \in H^0(\Omega_S)$, we have

$$\begin{aligned}\mathcal{F}(v) &\equiv \int_{\Omega_S} f(x,y)v(x,y)\,dx\,dy \\ &= \int_{\hat{\Omega}_S} \beta_1\beta_2 e^{2\beta_1\eta}\,\hat{f}(\xi,\eta)\hat{v}(\xi,\eta)\,d\xi d\eta \equiv \hat{\mathcal{F}}(\hat{v}).\end{aligned} \tag{A.3}$$

Proof. Since, for the mapping size $\beta = (\beta_1, \beta_2)$, the inverse of the Jacobian matrix of the exponential auxiliary mapping is

$$\left[J\left(\varphi_{exp}^{\beta}\right)\right]^{-1} = \frac{1}{\beta_1\beta_2 e^{\beta_1\xi}}\begin{bmatrix}\beta_2\cos\beta_2\eta, & -\beta_1\sin\beta_2\eta \\ \beta_2\sin\beta_2\eta, & \beta_1\cos\beta_2\eta\end{bmatrix}, \tag{A.4}$$

$$\begin{aligned}\mathcal{B}(u,v) &= \int_{\hat{\Omega}_S} \left|J\left(\varphi_{exp}^{\beta}\right)\right|\left(\left[J\left(\varphi_{exp}^{\beta}\right)\right]^{-1}(\nabla_\xi\hat{u})^T\right)^T\begin{bmatrix} a_{11} & a_{12} \\ a_{21} & a_{22}\end{bmatrix}\left(\left[J\left(\varphi_{exp}^{\beta}\right)\right]^{-1}(\nabla_\xi\hat{v})^T\right)d\xi\,d\eta \\ &= \int_{\hat{\Omega}_S} \nabla_\xi\hat{u}\begin{bmatrix} c_{11} & c_{12} \\ c_{21} & c_{22}\end{bmatrix}(\nabla_\xi\hat{v})^T\,d\xi\,d\eta = \hat{\mathcal{B}}(\hat{u},\hat{v}). \quad \blacksquare\end{aligned} \tag{A.5}$$

By using a similar argument, we can prove the following lemma:

LEMMA AI.2. *Let $u, v \in H^1(\Omega_S)$, then by the power auxiliary mapping φ_{pow}^{β}, the bilinear form* (4) *and the linear functional* (5)*, are transformed to the following forms*:

$$\begin{aligned}\mathcal{B}(u,v) &\equiv \int_{\Omega_S} (\nabla_x u)\begin{bmatrix} a_{11} & a_{12} \\ a_{21} & a_{22}\end{bmatrix}(\nabla_x v)^T\,dx\,dy \\ &= \int_{\hat{\Omega}_S} (\nabla_\xi\hat{u})\begin{bmatrix} q_{11} & q_{12} \\ q_{21} & q_{22}\end{bmatrix}(\nabla_\xi\hat{v})^T\,d\xi\,d\eta \equiv \mathcal{B}^*(\hat{u},\hat{v}),\end{aligned} \tag{A.6}$$

where

$$\begin{cases} t = (1-\beta)\hat{\theta} \\ q_{11} = a_{11}\cos^2 t + a_{22}\sin^2 t - (a_{21}+a_{12})\sin t\cos t \\ q_{12} = (a_{11}-a_{22})\sin t\cos t - a_{21}\sin^2 t + a_{12}\cos^2 t \\ q_{21} = (a_{11}-a_{22})\sin t\cos t - a_{12}\sin^2 t + a_{21}\cos^2 t \\ q_{22} = a_{11}\sin^2 t + a_{22}\cos^2 t + (a_{12}+a_{21})\sin t\cos t. \end{cases}$$

For $v \in H^1(\Omega_S)$ and $f \in H^0(\Omega_S)$, we have

$$\begin{aligned} \mathcal{F}(v) &\equiv \int_{\Omega_S} f(x,y)v(x,y)\,dx\,dy \\ &= \int_{\hat{\Omega}_S} \beta^2(\xi^2+\eta^2)^{\beta-1}\hat{f}(\xi,\eta)\hat{v}(\xi,\eta)\,d\xi\,d\eta \equiv \mathcal{F}^*(\hat{v}). \end{aligned}$$

APPENDIX II

The Inequality for the Error Estimate

(PAM) Suppose the diameter of the neighborhood Ω_S of the singularity point is <1. Then, by (A1), we have $\max|J(\varphi^{\beta}_{pow})| \le \beta^2$ on $\hat{\Omega}_S$. Hence, we obtain the following inequalities:

$$\|u\|^2_{0,\Omega_S} = \int_{\Omega_S} |u|^2\,dx\,dy = \int_{\hat{\Omega}_S} \left|J\left(\varphi^{\beta}_{pow}\right)\right| \cdot |\hat{u}|^2\,d\xi\,d\eta \le \beta^2|\hat{u}|^2_{0,\hat{\Omega}_S}. \tag{A.7}$$

By applying (A.5) with the identity matrix in place of the coefficient matrix $[a_{ij}]$, we obtain

$$|u|^2_{1,\Omega_S} \equiv \int_{\Omega_S} (\nabla_x u)\cdot(\nabla_x u)^T\,dx\,dy = \int_{\hat{\Omega}_S} (\nabla_\xi \hat{u})\cdot(\nabla_\xi \hat{u})^T\,d\xi\,d\eta \equiv |\hat{u}|^2_{1,\hat{\Omega}_S}. \tag{A.8}$$

Since $\|u\|^2_1 = \|u\|^2_0 + |u|^2_1$, the equalities (A.7) and (A.8) imply the following inequality.

LEMMA AII.1. *For $u \in H^1(\Omega_S)$, we have*

$$\|u\|_{1,\Omega_S} \le \beta\|\hat{u}\|_{1,\hat{\Omega}_S}. \tag{A.9}$$

(EAM) Let us define a weighted Sobolev norm with respect to a weight function vector $W = (W_0, W_1)$ as follows:

$$\|v\|^2_{1,E,W} = \int_E (W_0|v|^2 + W_1\nabla v\cdot\nabla v). \tag{A.10}$$

The expression $H^1(\Omega; W) = \{v : \|v\|_{1,\Omega,W} < \infty\}$ is called a weighted Sobolev space with weight vector $W = (W_0, W_1)$.

We have the following equation:

$$\begin{aligned} \|u\|^2_{0,\Omega_S} &= \int_{\Omega_S} |u|^2\,dx\,dy = \int_{\hat{\Omega}_S} \left|J\left(\varphi^{\beta}_{exp}\right)\right| \cdot |\hat{u}|^2\,d\xi\,d\eta \\ &= \beta_1\beta_2 \int_{\hat{\Omega}_S} e^{\beta_1\xi}(\xi,\eta)|\hat{u}|^2\,d\xi\,d\eta. \end{aligned} \tag{A.11}$$

By applying (A.1) with identity matrix in place of the coefficient matrix $[a_{ij}]$, we have

$$|u|_{1,\Omega_S} \equiv \int_{\Omega_S} (\nabla_x u) \cdot (\nabla_x u)^T \, dx\, dy$$
$$= \int_{\hat{\Omega}_S} (\nabla_\xi \hat{u}) \cdot \begin{bmatrix} A & B \\ B & C \end{bmatrix} \cdot (\nabla_\xi \hat{u})^T \, d\xi\, d\eta, \tag{A.12}$$

where

$$\begin{cases} A = \frac{\beta_2}{\beta_1} \cos^2 \beta_2\eta + \frac{\beta_1}{\beta_2} \sin^2 \beta_2\eta, \\ B = 0.5 \sin(2\beta_2\eta) \cdot (\beta_2/\beta_1 - \beta_1/\beta_2), \\ C = \frac{\beta_2}{\beta_1} \sin^2 \beta_2\eta + \frac{\beta_1}{\beta_2} \cos^2 \beta_2\eta. \end{cases}$$

Let $M = \max\{\frac{\beta_2}{\beta_1}, \frac{\beta_1}{\beta_2}, |\frac{\beta_2}{\beta_1} - \frac{\beta_1}{\beta_2}|\}$, then by using the inequality: $2ab \le (a^2 + b^2)$, one can easily show that (A.11) is bounded by

$$|u|^2_{1,\Omega_S} \le 2M \int_{\hat{\Omega}_S} (\nabla_\xi \hat{u}) \cdot (\nabla_\xi \hat{u})^T \equiv 2M |\hat{u}|^2_{1,\hat{\Omega}_S}. \tag{A.13}$$

Thus, the inequalities (A.10) and (A.13) imply the inequality (A.14) of the following lemma.

LEMMA AII.2. *For $u \in H^1(\Omega_S; W = (e^{\beta_1\xi}, 1))$, if we let $K = \max\{\sqrt{\beta_1\beta_2}, \sqrt{2\beta_1/\beta_2}, \sqrt{2\beta_2/\beta_1}\}$, then*

$$\|u\|_{1,\Omega_S} \le K \|\hat{u}\|_{1,\hat{\Omega}_S,W}. \tag{A.14}$$

If $(\beta_1, \beta_2) = (1, 1)$ for the mapping size of the EAM, we have $K = \beta$. Moreover, since $\beta_1 > 0$ and $0 < \beta_2 \le 1$ in practice, K is actually $\sqrt{2\beta_1/\beta_2}$.

APPENDIX III

The Singular Elemental Mapping Constructed through EAM

Without loss of generality, we will work with the case where the mapping size is $\beta_1 = \beta_2 = 1$ and $\Omega_S = \{(r, \theta) : r < 1\}$. The infinite triangular elements of $\hat{\Omega}_S$ in Fig. 7 are denoted by $\hat{T}_1^\infty = \overline{2 \to 3 \to 1}, \ldots, \hat{T}_8^\infty = \overline{10 \to 2 \to 1}$, and the quadrilateral elements of $\hat{\Omega}_S$ in Fig. 7 are denoted by $\hat{Q}_9 = \overline{3 \to 2 \to 11 \to 12}, \ldots, \hat{Q}_{24} = \overline{11 \to 19 \to 28 \to 20}$. Let $(X_1, Y_1) = (0, 0), (X_2, Y_2), (X_3, Y_3), \ldots, (X_{37}, Y_{37})$ are the coordinates of the nodes $1, 2, 3, \ldots, 37$ of the mesh of Ω_S in Fig. 7, respectively. The coordinates of the corresponding points in $\hat{\Omega}_S$ are denoted by $(\hat{X}_k, \hat{Y}_k) = [\varphi^1_{exp}]^{-1}(X_k, Y_k), k = 1, 2, \ldots, 37$, respectively.

(III.1) The elemental mappings from $\Omega^{(t)}_{st}$ onto the infinite triangular elements of $\hat{\Omega}_S$: By using a similar method to that in [25], the elemental mapping $\hat{\Psi}_1^\infty$ from the reference triangular element $\Omega^{(t)}_{st} - \{(0, \sqrt{3})\}$ onto the infinite triangular element $\hat{T}_1^\infty$ is constructed as the composition of the following two mappings. That is, $\hat{\Psi}_1^\infty(\xi_t, \eta_t) = (H_1 \circ H_0)(\xi_t, \eta_t)$, where $H_0 : \Omega^{(t)}_{st} - \{(0, \sqrt{3})\} \to \Omega^{(q)}_{st}$ is defined by

$$H_0(\xi_t, \eta_t) = \left(\frac{\sqrt{3}\xi_t}{\sqrt{3} - \eta_t}, \frac{2\eta_t}{\sqrt{3}} - 1 \right),$$

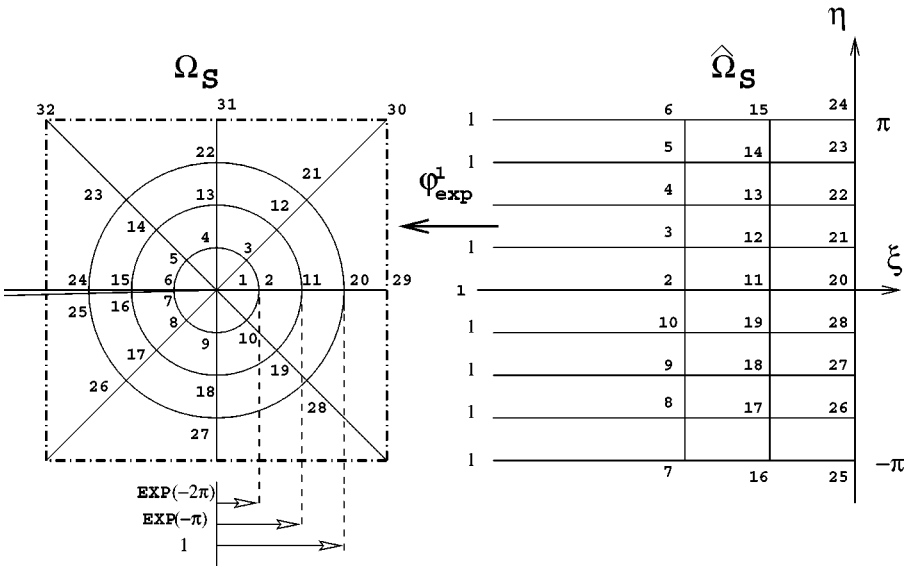

FIG. 7. Scheme of Neighborhood Ω_S of crack tip and the Mapped Neighborhood $\hat{\Omega}_S$ by the exponential auxiliary mapping φ^{β}_{exp} when the map size vector is $\beta = (1, 1)$.

and $H_1 : \Omega^{(q)}_{st} \to \hat{T}^{\infty}_1$ is defined by

$$H_1(\xi_t, \eta_t) = \left(\frac{-\eta_t}{1-\eta_t}(\hat{X}_2 + \hat{X}_{11}) + \frac{1}{1-\eta_t}(\hat{X}_2 - \hat{X}_{11}), \frac{1-\xi_t}{2}\hat{Y}_2 + \frac{1+\xi_t}{2}\hat{Y}_3 \right).$$

The elemental mappings from $\Omega^{(t)}_{st} - \{(0, \sqrt{3})\}$ onto all other infinite triangular elements $\hat{T}^{\infty}_k$, $k = 2, \ldots, 8$, are defined in a similar manner.

(III.2) The elemental mappings from $\Omega^{(q)}_{st}$ onto the quadrilateral elements of $\hat{\Omega}_S$: The elemental mappings from the reference quadrilateral element $\Omega^{(q)}_{st}$ onto the quadrilateral elements of $\hat{\Omega}_S$ are the standard polynomial mappings.

(III.3) The elemental mappings from $\Omega^{(q)}_{st}$ onto the quadrilateral elements with one curved side in Fig. 7: Because of the specified mesh near the crack in Fig. 7, the mesh on Ω has eight quadrilateral elements with one curved side. Then a blending type elemental mapping from $\Omega^{(q)}_{st}$ onto the curved quadrilateral element Q_k is constructed by using the method in Chapter 6 of [23].

Now for the eight triangular elements with one curved side and 16 quadrilateral elements with two curved sides, we construct singular elemental mappings as follows: for $1 \le k \le 8$,

$$\Psi^S_k = \varphi^{(1,1)}_{exp} \circ \hat{\Psi}^{\infty}_k : \Omega^{(t)}_{st} \to T_k \equiv \varphi^{(1,1)}_{exp}\left(\hat{T}^{\infty}_k\right) \tag{A.15}$$

and for $9 \le k \le 24$,

$$\Psi^S_k = \varphi^{(1,1)}_{exp} \circ \hat{\Psi}_k : \Omega^{(q)}_{st} \to Q_k \equiv \varphi^{(1,1)}_{exp}(\hat{Q}_k). \tag{A.16}$$

Let us note

1. Unlike the standard polynomial type elemental mappings, the inverses of the elemental mappings Ψ^S_k, constructed through the exponential auxiliary mapping, are singular for $k \le 24$.

2. The singular elemental mappings $\Psi_{17}^S, \ldots, \Psi_{24}^S$ and the blending type elemental mappings $\Psi_{25}, \ldots, \Psi_{32}$, defined above are linearly changing in ξ_t along the common circular sides between Q_{17} and Q_{25}, Q_{18} and Q_{26}, and so on. Thus, the finite element space constructed through these elemental mappings is "exactly conforming."

ACKNOWLEDGMENTS

The authors thank Professor Benqi Guo of the University of Manitoba for his helpful comments and constructive suggestions.

REFERENCES

1. B. Anderson, U. Falk, I. Babuška, and T. V. Petersdorff, Reliable Stress and Fracture Mechanics Analysis of Complex Components Using a h-p Version of FEM, *Int. J. Numer. Meth. Engng.* **38**, 2135 (1995).
2. I. Babuška, B. Anderson, B. Guo, J. Melenk, and H.-S. Oh, Finite element method for solving problems with singular solutions, *J. Comput. Appl. Math.* **74**, 51 (1996).
3. I. Babuška and B. Guo, The h-p version of the finite element method for domains with curved boundaries, *SIAM J. Numer. Anal.* **25**, 837 (1988).
4. I. Babuška and B. Guo, Direct and inverse approximation theorems for the p version of the finite element method in the frame of weighted besov spaces, part I: In two dimensions. Submited for publication.
5. I. Babuška and H.-S. Oh, The p-version of the finite element method for domains with corners and for infinite domains, *Number. Meth. PDEs* **6**, 371 (1990).
6. I. Babuška and M. R. Rosenzweig, A finite element scheme for domains with corners, *Numer. Math.* **20**, 1 (1972).
7. I. Babuška and M. Suri, The optimal convergence rate of the p-version of the finite element method, *SIAM J. Numer. Anal.* **24**, 750 (1987).
8. I. Babuška and M. Suri, The h-p version of the finite element method with quasi-uniform meshes, *Math. Modelling and Numer. Anal.* **21**, 199 (1987).
9. W. Gordon and C. Hall, Construction of curvilinear co-ordinate systems and applications to mesh generation, *Int. J. Numer. Meth. Eng.* **7**, 461 (1973).
10. P. Grisvard, *Elliptic Problems in Nonsmooth Domains* (Pitman, 1985).
11. B. Guo and H.-S. Oh, The h-p version of the finite element method for problems with interfaces, *Int. J. Numer. Meth. Eng.* **37**, 1741 (1994).
12. J. A. Hendry and L. M. Delves, Global element method applied to a harmonic mixed boundary value problem, *J. Comp. Phys.* **33**, 33 (1979).
13. S. J. Lee, H.-S. Oh, and J. H. Yun, Extension of the method of auxiliary mapping for three-dimensional elliptic boundary value problems, *Int. J. Numer. Meth. Eng.* **50**, 1103 (2001).
14. T. R. Lucas and H.-S. Oh, The method of auxiliary mappings in the finite element solutions of elliptic boundary problems containing singularities, *J. Comp. Phys.* **108**, 327 (1993).
15. J. M. Melenk and I. Babuška, Partition of unity finite element method: basic theory and applications, *Comp. Meth. Applied Mech. Eng.* **139**, 289 (1996).
16. H.-S. Oh, Highly accurate mode separated energy release rates for delamination cracks, *Proceedings of the NINTH United States–Japan Conference on Composite Materials*, 2000, pp. 299–306.
17. H.-S. Oh and I. Babuška, The p-version of the Finite Element Method for Elliptic Boundary Value Problems with Interfaces, *Comp. Meth. Applied Mech. Eng.* **97**, 211 (1992).
18. H.-S. Oh and I. Babuška, The Method of Auxiliary Mapping For the Finite Element Solutions of Plane Elasticity Problems Containing Singularities, *J. Comp. Phys.* **121**, 193 (1995).
19. V. Z. Parton and P. I. Perlin, *Mathematical Methods of the Theory of Elasticity, Volume 1* (Mir, Moscow, 1984).

20. J. Schön and B. Anderson, Interaction between a delamination crack and a matrix crack, *Proceedings of the 13th Annual Technical Conference on Composite Materials*, edited by A. J. Vizzini (American Society for Composites, 1998).
21. J. Schön and B. Anderson, Calculation of mode-separated energy release rates during delamination growth, *Proceedings of the 13th Technical Conference on Composite Materials*, edited by A. J. Vizzini (American Society for Composites, 1998).
22. G. Strang and G. Fix, *An Analysis of the Finite Element Method* (Prentice Hall, New York, 1973).
23. B. Szabó and I. Babuška, *Finite Element Analysis* (Wiley, New York, 1990).
24. G. Tsamasphyros, Singular element construction using a mapping technique, *Int. J. Numer. Meth. Eng.* **24**, 1305 (1987).
25. O. C. Zienkiewicz, K. Bando, K. Bettess, C. Emson, and T. C. Chiam, Mapped Infinite Elements for Exterior Wave Problems, *Int. J. Numer. Meth. Eng.* **21**, 1229 (1985).